Carbohydrate Polymers 112 (2014) 595–602

Contents lists available at ScienceDirect

Carbohydrate Polymers

journal homepage: www.elsevier.com/locate/carbpol

Hydroxyethylcellulose used as an eco-friendly inhibitor for 1018 c-steel corrosion in 3.5% NaCl solution

Mahmoud N. EL-Haddad *

Chemistry Department, Faculty of Science, Mansoura University, P.O. Box: 35516, Mansoura, Egypt

ARTICLE INFO

Article history:
Received 8 May 2014
Received in revised form 23 May 2014
Accepted 13 June 2014
Available online 19 June 2014

Keywords:
Carbon steel
Polarization
EIS
SEM
Kinetic parameters

ABSTRACT

The inhibition effect of hydroxyethylcellulose (HEC) on 1018 c-steel corrosion in 3.5% NaCl solution was investigated by using potentiodynamic polarization, electrochemical frequency modulation (EFM) and electrochemical impedance spectroscopy (EIS) techniques. The potentiodynamic polarization studies suggested that HEC acts as a mixed-type inhibitor. Data obtained from EIS were analyzed to model the corrosion inhibition process through equivalent circuit. Results obtained from EFM technique were shown to be in agreement with potentiodynamic and EIS techniques. The adsorption behavior of HEC on steel surface follows the Langmuir adsorption isotherm. Thermodynamic parameter (ΔG°_{ads}) and activation parameters (E_a^*, ΔH^* and ΔS^*) were calculated to investigate mechanism of inhibition. Scanning electron microscopy (SEM) and energy dispersive X-ray (EDX) analysis system were performed to characterize the film formed on the metal surface. *DMol*^{3} quantum chemical calculations were performed to support the adsorption mechanism with the structure of HEC molecule.

1. Introduction

The corrosion inhibition of 1018 c-steel becomes of such interest because it is widely used as a constructional materials in many industries, and this is due to its excellent mechanical properties and low cost. To prevent the base metal attack during these processes, corrosion inhibitors are widely used. It is reported that organic materials such as polymers or macromolecules, having functional groups (—OH, —COOH, —NH_2, etc.), are found to be corrosion inhibitors in different corrosive media (Ashassi-Sorkhabi & Ghalebsaz-Jeddi, 2005; Baoa, Zhanga, & Wan, 2011; Cheng, Chen, Liu, Chang, & Yin, 2007; Deng, Li, & Xie, 2014; El-Haddad, 2013; El-Sayed, 1996; Fekry & Mohamed, 2010; Müller, Förster, & Kläger, 1997; Sathiyanarayanan, Balakrishnan, Dhawan, & Trivedi, 1994; Solomon & Umoren, 2010; Umoren, Solomon, Udosoro, & Udoh, 2010; Waanders, Vorster, & Geldenhuys, 2002). Larger corrosion inhibition efficiencies that are observed using polymers are not only due to the presence of π-electrons but it can be also attributed to the larger molecular size which ensures greater coverage of metallic surface (Sathiyanarayanan et al., 1994). HEC is water soluble polymer derived from cellulose, relatively cheap, non-toxic, eco-friendly corrosion inhibitor. It has wide spread applications as a binder, thickener, stabilizer, suspension and water retaining agent in food industry, pharmaceutical, cosmetic, paper and other industrial areas (WHO, 1998). HEC has been reported to inhibit the corrosion of aluminum and mild steel in HCl solution (Arukalam, 2012). In the present work the corrosion inhibiting behavior of HEC on 1018 c-steel corrosion in 3.5% NaCl solution have been investigated using potentiodynamic polarization, electrochemical frequency modulation (EFM) and electrochemical impedance spectroscopy (EIS) techniques. The surface of 1018 c-steel was analyzed using scanning electron microscopy (SEM) and energy dispersive X-ray (EDX) analysis system to confirm the compositions of the corrosion products formed on the surface. *DMol*^{3} quantum chemical calculations were also employed to discuss the correlation of inhibition efficiency and molecule structure of HEC.

2. Experimental

2.1. Materials and solutions

The chemical composition of 1018 c-steel used in this investigation is the following (mass %): C – 0.20, Mn – 0.35, Si – 0.003, P – 0.024 and rest Fe. The steel sheet is cut into coupons of dimension 1.0 cm × 1.0 cm × 0.8 cm. The coupon was embedded in epoxy resin in a glass tube. A copper wire was soldered to the rear side of the coupon as an electrical connection. The exposed surface area of the electrode (0.5 cm^2) was abraded with a series of emery papers up

* Tel.: +20 1006423871.
E-mail address: noaman_eg@yahoo.com

http://dx.doi.org/10.1016/j.carbpol.2014.06.032

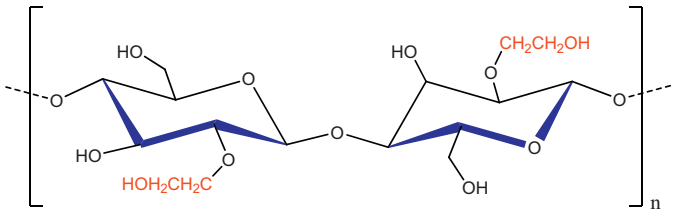

Fig. 1. Chemical structure of HEC repeat unit.

to 1200 grade. The electrode was then rinsed with distilled water and ethanol to remove possible residue of polishing and air dried. This was used as the working electrode during the electrochemical methods. Testing electrolyte was 3.5% NaCl solution diluted in distilled water, used as blank solution. The inhibitor hydroxyethylcellulose (HEC) was purchased from Sigma–Aldrich Co., and chemical structure of the repeat unit is presented in Fig. 1. The concentration range of HEC used in this work was 0.1–0.5 mM.

2.2. Electrochemical experiments

The electrochemical measurements were performed in a typical three-compartment glass cell consisted of the 1018 c-steel specimen as working electrode (WE), platinum electrode as auxiliary electrode (AE), and a saturated calomel electrode (SCE) as the reference electrode (RE). The experiments were preformed using a Gamry instrument Potentiostat/Galvanostat/ZRA (PCI4G750) connected with a personal computer; these include Gamry framework system based on the ESA400. Various electrochemical parameters were simultaneously determined using dc105 corrosion software, EFM140 software and EIS300 impedance software. Echem Analyst 5.5 software was used for collecting, fitting and plotting the data. Each run was carried out in aerated solutions at the required temperature, using a water thermostat. All given potentials were referred to SCE. The working electrode was immersed in the test solution for 30 min until the open potential circuit potential (E_{OC}) reached. The potentiodynamic current–potential curves were carried out at a scan rate 1.0 mV s^{-1}, and the potential was started from (−1200 mV up to +200 mV) versus open circuit potential. EFM carried out using two frequencies 2.0 and 5.0 Hz. The base frequency was 1.0 Hz. We use a perturbation signal with amplitude of 10 mV for both perturbation frequencies of 2.0 and 5.0 Hz (Bosch, Hubrecht, Bogaerts, & Syrett, 2001; Khaled, 2008). EIS measurements were carried out using AC signals of amplitude 10 mV peak to peak at the open-circuit potential in the frequency range 100–50 kHz.

2.3. Quantum chemical calculations

The molecule sketch of HEC was drawn by ChemBio Draw Ultra 12.0. Then the quantum chemical calculations were performed using *DMOL*^{3} method in Materials Studio package (Materials Studio, 2009). *DMOL*^{3} is designed for the realization of large scale density functional theory (DFT) calculations. DFT semi-core pseudopods calculations (dspp) were performed with the double numerical basis sets plus polarization functional (DNP) to obtain the optimized geometry. Then the molecule's frontier orbital was expressed as relative density distribution figure.

2.4. SEM and EDX examination

Specimens of 1018 c-steel were immersed in 3.5% NaCl solution without and with HEC (0.5Mm) for 2 days at 25 °C. After that, the surface of test coupons examined using a scanning electron microscope (SEM, JOEL, JSM-T20, Japan) and an X-ray diffractometer

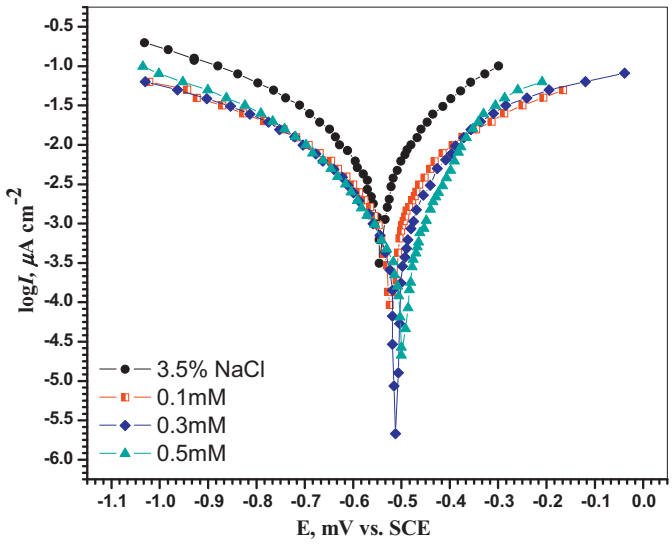

Fig. 2. Potentiodynamic polarization curves for 1018 c-steel in 3.5% NaCl in absence and presence of various concentrations of HEC at 25 °C.

Philips (pw-1390) with Cu-tube (Cu Kα1, l = 1.54051 Å) analysis system.

3. Results and discussion

3.1. Electrochemical measurements

3.1.1. Potentiodynamic polarization

Potentiodynamic polarization curves for 1018 c-steel in 3.5% NaCl in absence and presence of different concentrations of HEC at 25 °C are shown in Fig. 2. Tafel slopes (β_a, β_c) and corrosion current density (I_{corr}), obtained by extrapolation of the Tafel lines. The percentage inhibition efficiency (ε_p%) and the degree of surface coverage (θ), were calculated from the following equation (Sahin, Gece, Karc, & Bilgic, 2008):

$$\varepsilon_p\% = \theta \times 100 = \left[1 - \frac{I_{inh}}{I_b}\right] \times 100 \quad (1)$$

where I_b and I_{inh} are the corrosion current densities in the absence and the presence of the inhibitor, respectively. As shown from Fig. 2, anodic and cathodic current density (I_{corr}) decreased with the increase in inhibitor concentration, so inhibition efficiency (ε_p) increased. This due to that, the addition of inhibitor reduces anodic dissolution of metal and also retards evolution of hydrogen reaction. This effect is duo to the adsorption of inhibitor on the active centers of steel surface (Singh & Quraishi, 2010). The corrosion parameters, evaluated from Tafel polarization curves are listed in Table 1. It was found that (Table 1), the slopes of the cathodic and anodic Tafel lines are approximately constant and independent on the inhibitor concentration. This behavior suggests that the inhibitor molecules have no effect on the metal dissolution mechanism. In addition, the values of (E_{corr}) do not change significantly in the presence of inhibitor. So, HEC acts as a mixed type inhibitor (El-Haddad & Elattar, 2012).

3.1.2. Electrochemical frequency modulation (EFM)

The EFM technique is used to calculate the anodic and cathodic Tafel slopes as well as corrosion current densities without prior knowledge of Tafel constants. EFM is a non-destructive technique and is a rapid test. Fig. 3a and b shows representative examples for EFM intermodulation spectra of 1018 c-steel in 3.5% NaCl solutions devoid of and containing 0.5 mM HEC at 25 °C. Similar results were recorded for the other concentrations. Each spectrum is a current

Table 1
Electrochemical parameters evaluated from potentiodynamic polarization measurements for 1018 c-steel in 3.5 NaCl in the absence and presence of various concentrations of HEC at 25 °C.

Inhibitor Conc. (mM)	$-E_{corr}$ (mV)	i_{corr} ($\mu A\,cm^{-2}$)	β_c ($mV\,dec^{-1}$)	β_a ($mV\,dec^{-1}$)	θ	ε_p%
–	542	12.23	391	335	–	–
0.1	537	1.377	212	174	0.887	88.7
0.3	531	1.091	203	163	0.911	91.1
0.5	533	0.955	182	143	0.967	96.7

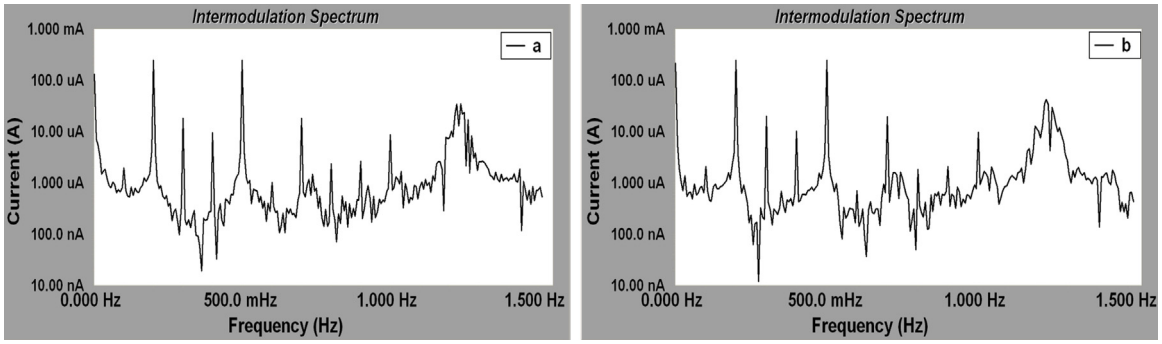

Fig. 3. Intermodulation spectra of 1018 c-steel in 3.5% NaCl solution (a), and intermodulation spectra of 1018 c- steel in 3.5% NaCl solution in presence of 0.5 mM HEC (b) at 25 °C.

response as a function of frequency. The peaks of spectrum are analyzed by the EFM140 software package to calculate the corrosion current and the Tafel constants. The inhibition efficiency (ε_{EFM}%) and the degree of surface coverage (θ) can be calculated from the following equation:

$$\varepsilon_{EFM}\% = \theta \times 100 = \left[1 - \frac{I_{inh}}{I_b}\right] \times 100 \quad (2)$$

The calculated electrochemical parameters (I_{corr}, β_a, β_c CF2, CF3 and ε_{EFM}%) are given in Table 2. It is obvious from Table 2 that, (I_{corr}) values decrease, while those of (ε_{EFM}%) increase with increase in the inhibitor concentration, indicating that HMC inhibits the corrosion of metal through adsorption. The values of causality factors (CF2, CF3) are approximately equal the theoretical values (2) and (3) according to the EFM theory, indicating that, the validity of Tafel slopes and corrosion current densities (Abdel Rehim, Hazzazi, Amin, & Khaled, 2008; Amin, Abd El Rehim, & Abdel-Fatah, 2009).

3.1.3. Electrochemical impedance spectroscopy (EIS)

EIS measurements were carried out at the respective corrosion potentials after 30 min of immersion of 1018 c-steel in uninhibited and inhibited solutions of 3.5% NaCl. Fig. 4 shows Nyquist plots (a) and Bode plots (b) of 1018 c-steel in uninhibited and inhibited 3.5% NaCl solutions containing various concentrations of HEC at 25 °C. The Nyquist plots shows single capacitive loop, both in uninhibited and inhibited solutions and the diameter of the capacitive loop increases on increasing the inhibitor concentration indicating that, the corrosion inhibition of steel. It is found that the obtained Nyquist plots are not yield perfect semicircles due to the frequency dispersion, as well as electrode surface heterogeneity resulting from surface roughness, impurities, adsorption of inhibitors and formation of porous layers (Growcock & Jasinski, 1989; Machnikoval, Pazderova, Bazzaoui, & Hackerman, 2008; Paskossy, 1994). A Nyquist plots does not show any frequency value although some definite frequency was used to get the impedance at each data point. To overcome this shortcoming, a Bode plot was developed to indicate exactly what frequency was used to create a data point. The experimental data fitted using the electrical

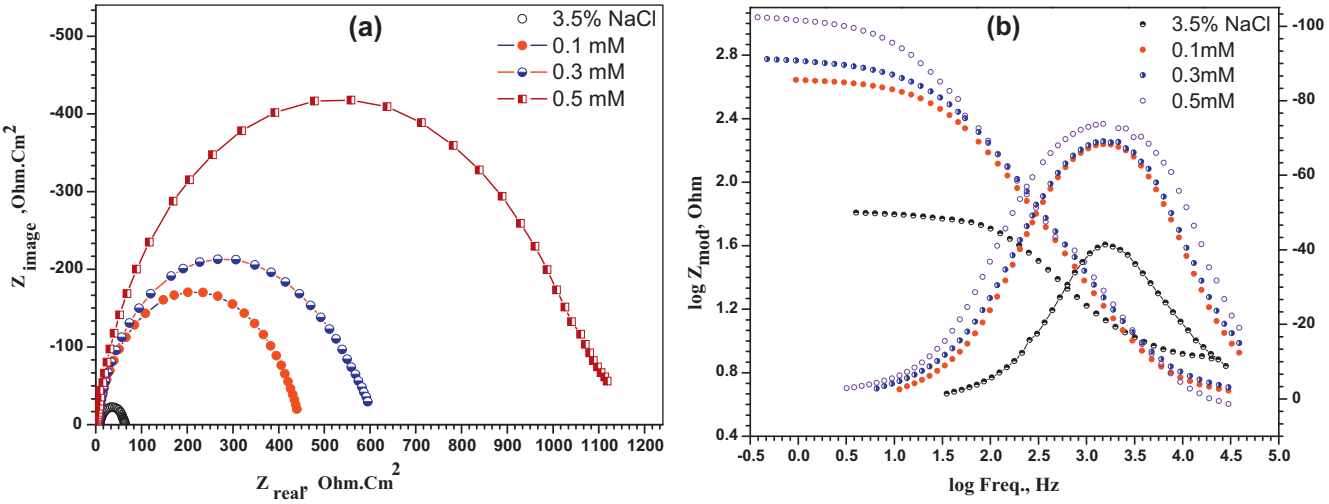

Fig. 4. Nyquist plots (a) and Bode plots (b) of 1018 c-steel in uninhibited and inhibited 3.5% NaCl solutions containing various concentrations of HEC at 25 °C.

Table 2
Electrochemical parameters evaluated from electrochemical frequency modulation (EFM) measurements for 1018 c-steel in 3.5 NaCl in the absence and presence of various concentrations of HEC at 25 °C.

Inhibitor Conc. (mM)	i_{corr} (μA cm^{-2})	β_c (mV dec^{-1})	β_a (mV dec^{-1})	CF-2	CF-3	θ	ε_{EFM}%
–	15.65	384	330	1.9	2.8	–	–
0.1	2.35	2.17	187	2.1	2.9	0.849	84.9
0.3	1.52	210	176	1.9	3.2	0.902	90.2
0.5	0.81	197	168	2.2	2.9	0.948	94.8

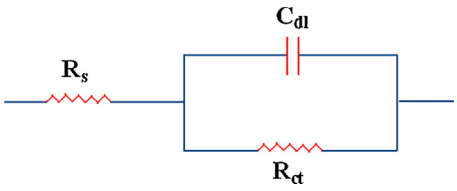

Fig. 5. Electrical equivalent circuit (R_s, solution resistance; R_{ct}, charge transfer resistance; C_{dl}, double layer capacitance) used in fitting the experimental impedance data.

equivalent circuit, which are given in Fig. 5 (Zhou, Lu, Xin, Liu, & Zhang, 2014). In this circuit, R_s and R_{ct} represent the solution resistance between the steel electrode and the reference electrode and the charge-transfer resistance corresponding with the corrosion reaction at metal substrate/solution interface, respectively. The double layer capacitance C_{dl} is placed in parallel to the charge transfer resistance R_{ct} due to the charge transfer reaction (Wu, Ma, & Chen, 1999). The double layer capacitance values (C_{dl}) at different inhibitor concentrations, is calculated according to the following equation (Benchikh, Aitout, Makhloufi, Benhaddad, & Saidani, 2009):

$$C_{dl} = \frac{1}{\omega R_{ct}} = \frac{1}{2\pi \int_{max} R_{ct}} \quad (3)$$

where (ω) is the angular frequency and $\int_{max}$ is the frequency at the apex of the first capacitive loop. The semicircles at high frequencies in Fig. 4 are associated with the electrical double layer capacitors (C_{dl}) and the diameters of the high frequency semicircles can be considered as the charge-transfer resistance (R_{ct}) (Ma et al., 2002). So, the inhibition efficiency, (ε_{EIS}%) and the degree of surface coverage (θ) of HEC can be calculated from the charge-transfer resistance as the following equation (El-Haddad, 2013):

$$\varepsilon_{EIS}\% = \theta \times 100 = \left[1 - \frac{R^*_{ct}}{R_{ct}}\right] \times 100 \quad (4)$$

where R^*_{ct} and R_{ct} are the charge-transfer resistances for uninhibited and inhibited solutions, respectively. The various parameters derived from EIS measurements and inhibition efficiencies are given in Table 3.

As seen from Table 3, the R_s values are very small compared to the R_{ct} values. The R_{ct} values tend to increase with the increase of inhibitor concentration, so that the ε_{EFM}% increased. This indicates that the inhibitor molecules have the capability of forming uniform compact adsorbed layer over metal electrode (Benchikh et al., 2009). On the other hand, the values of C_{dl} are decreased with increase in inhibitor concentration, are due to a reduction in local dielectric constant and/or increase in thickness of the electrical double layer, suggested that HEC molecules inhibit the metal corrosion via adsorption at the metal/solution interface (Quraishi & Rawat, 2001).

Table 3
Electrochemical parameters evaluated from electrochemical impedance spectroscopy (EIS) measurements for 1018 c-steel in 3.5 NaCl in the absence and presence of various concentrations of HEC at 25 °C.

Inhibitor Conc. (mM)	R_{ct} (Ω cm^2)	C_{dl} (μF cm^{-2})	θ	ε_{EIS} (%)
–	50.45	14.26	–	–
0.1	341	8.461	0.852	85.2
0.3	818	6.775	0.938	93.8
0.5	1368	5.137	0.963	96.3

3.2. Adsorption isotherm and thermodynamic parameters

In order to gain more information about the adsorption mode of HEC on the metal surface, the experimental data have been tested with several adsorption isotherms including Langmuir, Temkin, Frumkin and Flory–Huggins. In order to obtain the isotherm, the values of surface coverage (θ) were calculated from the from EFM data as the following equation (Chen et al., 2012):

$$\theta = \frac{\varepsilon_{EFM}\%}{100} \quad (5)$$

The best correlation between the experimental results and isotherm functions was obtained using Langmuir adsorption isotherm. According to this isotherm, θ is related to inhibitor concentration (C_{inh}) by the following equation (Li, Deng, & Fu, 2009):

$$\frac{C_{inh}}{\theta} = \frac{1}{K_{ads}} + C_{inh} \quad (6)$$

where K_{ads} is the adsorption equilibrium constant. The plots of (C/θ) vs. (C_{inh}) yield straight line with nearly unit slope and the linear correlation coefficient (R^2) is almost equal to 1 (R^2 = 0.998), suggesting that the adsorption of HEC on the metal obeys the Langmuir adsorption isotherm as presented in Fig. 6. The intercept permits the calculation of the equilibrium constant (K_{ads}) which is equals 56.08525 M^{-1}. The high value of K_{ads} implies more adsorption than desorption and consequently better inhibition efficiency (Refaey, Taha, & Abd El-Malak, 2004). K_{ads} is related to the standard free

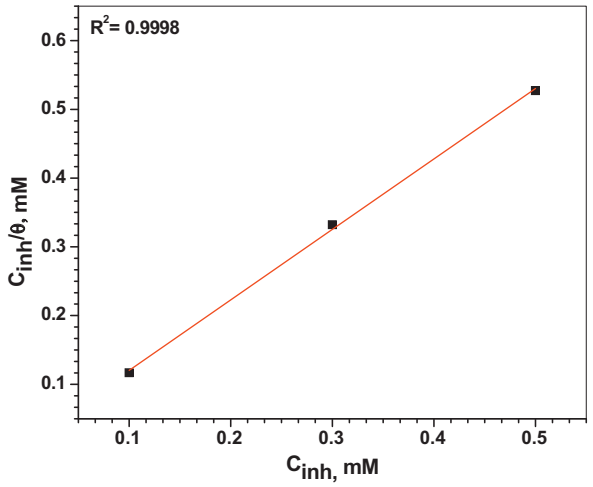

Fig. 6. Langmuir's adsorption plots of 1018 c-steel in 3.5 NaCl and containing various concentrations of HEC at 25 °C.

Table 4
The effect of various temperatures on the inhibition efficiency of 1018 c-steel corrosion in 3.5% NaCl solution in the absence and presence of various concentrations of HEC.

T (K)	Inhibitor Conc. (mM)	I_{corr} ($\mu A\,cm^{-2}$)	ε_p (%)
298	–	12.23	–
	0.1	1.377	88.7
	0.3	1.091	91.1
	0.5	0.955	95.5
308	–	14.45	–
	0.1	4.424	69.4
	0.3	3.824	73.5
	0.5	3.701	74.4
318	–	16.92	–
	0.1	8.250	51.2
	0.3	7.872	53.4
	0.5	6.821	59.7
328	–	18.85	–
	0.1	12.95	31.3
	0.3	11.252	40.3
	0.5	10.251	44.2

energy of adsorption (ΔG°_{ads}) as shown in the following equation (Ansari, Quraishi, & Singh, 2014):

$$K_{ads} = \frac{1}{55.5}\exp\left(-\frac{\Delta G^{\circ}_{ads}}{RT}\right) \quad (7)$$

where is the value of 55.5 being the concentration of water in solution expressed in mole, R is the universal gas constant and T is the absolute temperature. The standard free energy of adsorption (ΔG°_{ads}), which can characterize the interaction of adsorption molecules with metal surface, was calculated by Eq. (7) and is equal to $-19.9\,kJ\,mol^{-1}$. The negative value of ΔG°_{ads} indicates the spontaneous adsorption of HEC molecules from NaCl solution to the metal surface. It is well known that, the values of ΔG°_{ads} around $-20\,kJ\,mol^{-1}$or lower are associated with an electrostatic interaction between charged molecules and charged metal surface (physisorption); those of $-40\,kJ\,mol^{-1}$ or higher involve charge sharing or transfer from the inhibitor molecules to the metal surface to form a coordinate covalent bond (chemisorption) (Ehteshamzadeh, Shahrabi, & Hosseini, 2006). The value of ΔG°_{ads} in our experiment is less than $-40\,kJ\,mol^{-1}$, indicated that physical adsorption. In addition to electrostatic interaction, there may be molecular interaction (Obot, Obi-Egbedi, & Umoren, 2009).

3.3. Effect of temperature and kinetic parameters

The effect of temperature on the inhibition effect of HEC on 1018 c-steel corrosion was studied by polarization method. In this study, different concentrations of the inhibitor were used at different temperatures are given in Table 4. It was found that (Table 4), the (I_{corr}) increased with increasing temperature in the absence and presence of various concentrations of inhibitor in 3.5% NaCl solutions, but the (ε_p%), decreased with increasing temperature. This behavior can be related to the weakness of HEC adsorption on the metal surface at higher temperatures and suggests a physical adsorption of inhibitor on the metal surface (Ashassi-Sorkhabi & Ghalebsaz-Jeddi, 2005). The activation parameters were calculated from Arrhenius equation and transition state equation (del Campo, Perez-Saez, Gonzalez-Fernandez, & Tello, 2009; Karakus, Sahin, & Bilgiç, 2005):

$$I_{corr} = ke^{(-(E_a^*/RT))} \quad (8)$$

$$I_{corr} = \frac{RT}{Nh}e^{((\Delta S^*/R)-(\Delta H^*/RT))} \quad (9)$$

Table 5
Kinetic parameters for 1018 c-steel in 3.5 NaCl in the absence and presence of various concentrations of HEC at 25 °C.

Inhibitor Conc. (mM)	E_a^* ($kJ\,mol^{-1}$)	ΔH^* ($kJ\,mol^{-1}$)	$-\Delta S^*$ ($J\,mol^{-1}\,k^{-1}$)
–	9.98	8.75	194.4
0.1	55.36	53.41	60.37
0.3	58.87	56.45	51.84
0.5	59.08	55.82	54.67

where I_{corr} is the current density, E_a^* is apparent effective activation energy, k is Arrhenius pre-exponential factor, h is Plank's constant, N the Avogadro's number, ΔS^* is the entropy of activation and ΔH^* is the enthalpy of activation. A plot of the logarithm of corrosion current density, $\log I_{corr}$ versus the reciprocal of absolute temperature, $1/T$ in absence and presence of various concentrations of inhibitor give straight line as shown in Fig. 7a. The values of E_a^* obtained from the slope of the lines are listed in Table 5. Fig. 7b showed the plot of $\log I_{corr}/T$ vs. $1/T$. Straight lines were obtained with a slope of $(-\Delta H^*/2.303R)$ and an intercept of, $\{\log(R/Nh) + \Delta S^*/2.303R\}$ from which the values of ΔH^* and ΔS^* have been calculated and listed in Table 5. It is found that, the values of E_a^* determined in solution containing inhibitor concentrations are higher than that of in absence of inhibitor is attributed to the physical adsorption of inhibitor on the metal surface. On the other hand, the higher values of E_a^* in the presence of inhibitor compared to that in its absence and the decrease of the (ε%) with temperature increase can be interpreted as an indication of physical adsorption (Umoren, 2008). The positive values of ΔH^* indicated that the corrosion process is endothermic one (Bentiss et al., 2007). On the other hand, the entropy of activation (ΔS^*) is negative in both in absence and presence of inhibitor, implying that the activated complex represented the rate determining step with respect to the association rather than the dissociation step. It means that a decrease in disorder occurred when proceeding from reactants to the activated complex (Abd El-Rehim, Hassan, & Amin, 2001).

3.4. Surface morphology by SEM/EDX

Fig. 8a–c shows the results of SEM images for 1018 c-steel in 3.5% NaCl in the absence (blank) and presence of 0.5 mM HEC inhibitor after immersion for 2 days at 25 °C, respectively. The morphology of specimen surface in the absence of HEC (Fig. 8a) shows that, a very rough surface was observed due to rapid corrosion attack of the metal in the corrosive solution. On the contrary, in the presence of the inhibitor (Fig. 8c), the rough surface is suppressed, due to the formation of an adsorbed protective film of the inhibitor on the metal surface (Badiea & Mohana, 2008; Okafor, Liu, & Zheng, 2009). Fig. 8b–d presents the EDX spectra for 1018 c-steel in 3.5% NaCl solution in the absence (blank) and presence of 0.5 mM HEC inhibitor after immersion for 2 days at 25 °C, respectively. The EDX spectra of steel in absence of HEC in 3.5% NaCl solution (Fig. 8b) shows the characteristics peaks of the elements constituting the 1018 c-steel sample. In presence of HEC (Fig. 8d), the intensities of C and O signals are enhanced. This enhancement in C and O signals is due to the carbon and oxygen atoms of the adsorbed HEC. Also, the same spectra show that the iron peaks observed in the presence of inhibitor are considerably suppressed relative to those observed in blank solution (Fig. 8b), and this suppression of the iron peaks, occurs because of the overlying inhibitor film (Amara, Braisaz, Villemin, & Moreau, 2008).

3.5. Molecular structure and inhibition mechanism

The optimized geometry of HEC molecule is shown in Fig. 9a. The adsorption of HEC on the steel surface in 3.5% NaCl solution

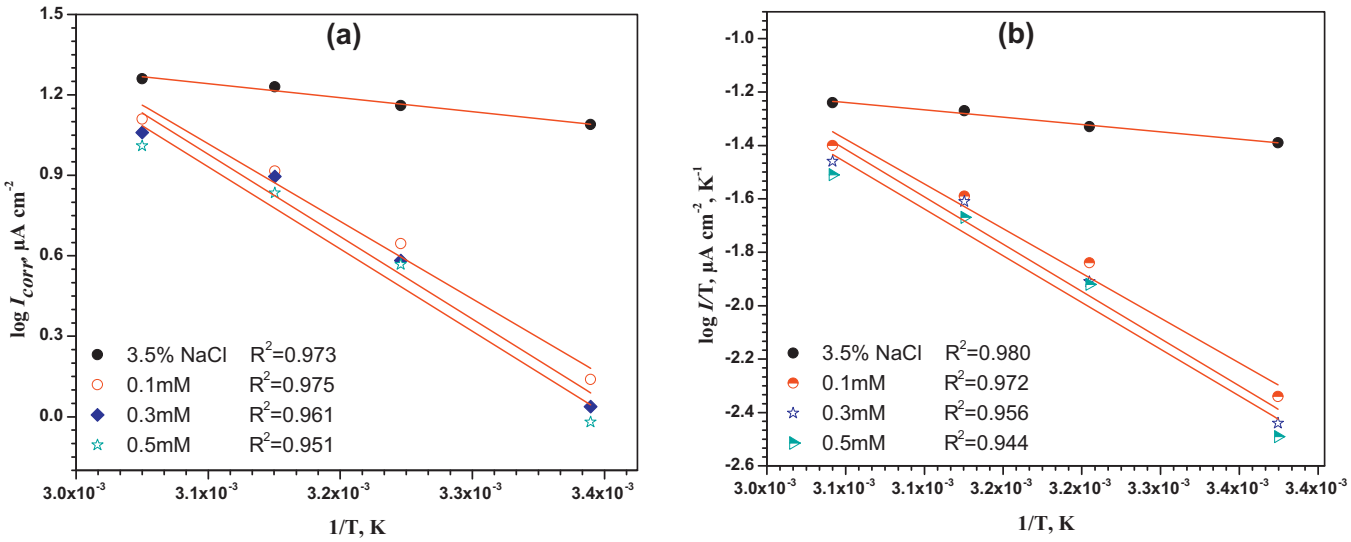

Fig. 7. Log I_{corr} versus $1/T$ (a) and log I_{corr}/T vs. $1/T$ (b) in absence and presence of various concentrations of HEC.

may be achieved by the interaction between the unshared electron pairs in oxygen with d-orbitals of iron atoms. The electron configuration of iron was [Ar] $4s^2 3d^6$, it is clear that, 3d orbit was not fully filled with electron. This unfilled orbital of iron could bond with the highest occupied molecular orbital (HOMO) of HEC while the filled 4s orbital could interact with the lowest unoccupied molecular orbital (LUMO) of the inhibitor (Li, Zhao, Liang, & Hou, 2005). The electronic orbital density distributions of HOMO and LUMO for HEC molecule are expressed in Fig. 9b–c. It can be observed that cycle A for the HOMO (see Fig. 9b), has larger electronic density and was more feasible to bind with 3d orbital of Fe; while for the LUMO (see Fig. 9c), cycle B, and C had larger orbital density and could take priority of interaction with 4s orbital of iron. From the geometry optimization of HEC, it can show that the oxygen atoms of inhibitor have Mulliken atomic charges with higher negative electron densities. This suggested that the oxygen atoms donate the unshared pair of electrons to the vacant d-orbitals of iron (Bereket, Gretir, & Yurt,

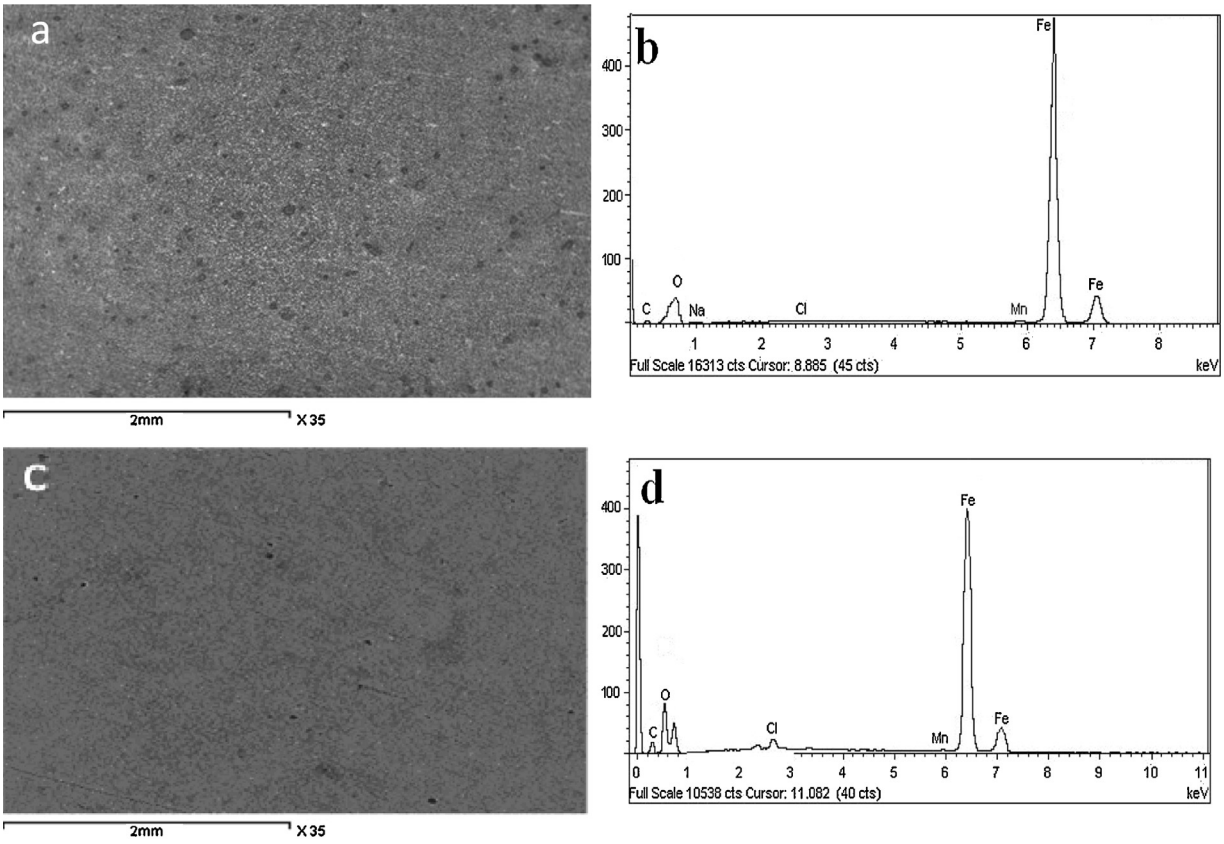

Fig. 8. SEM images and their corresponding EDX analysis of 1018 c-steel immersed for 2 days in (a and b) 3.5% NaCl solution, (c and d) 3.5% NaCl solution containing 0.5 mM HEC at 25 °C.

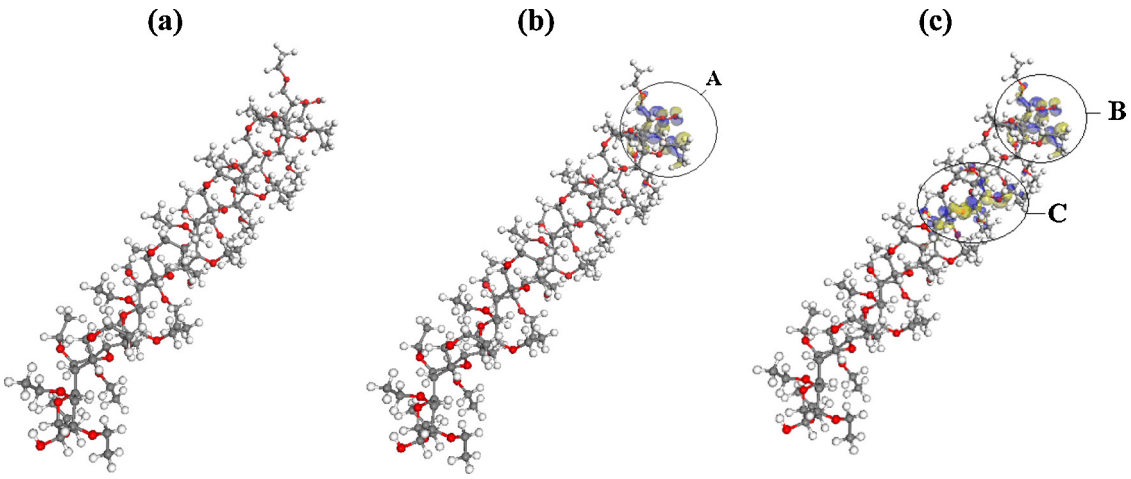

Fig. 9. Optimization geometry of HEC; (a), the molecule orbital of HEC that corresponds to bonding with iron atoms: (b) HOMO orbital density; (c) LUMO orbital density.

2001; Mulliken, 1955). So that, the active sites (oxygen atoms) facilitated the adsorption of inhibitor molecule on the surface of metal.

4. Conclusion

The corrosion inhibition of 1018 c-steel in 3.5% NaCl solution by hydroxyethylcellulose (HEC) as an eco-friendly inhibitor has been studied using electrochemical techniques, SEM and EDX analysis. The principle conclusions are:

- Results obtained from potentiodynamic polarization indicated that the HEC is mixed-type inhibitor.
- Results obtained from all electrochemical techniques are in good agreement.
- Adsorption of HEC on the steel surface is spontaneous and obeys the Langmuir's isotherm.
- Corrosion inhibition decreases when the temperature increases.
- SEM and EDX analysis of the steel surface showed that a film of inhibitor is formed on the steel surface. This film inhibited metal dissolution in 3.5% NaCl solution.
- *DMol*^{3} quantum chemical calculations were performed to support the adsorption mechanism with the structure of HEC molecule.

References

Abd El-Rehim, S. S., Hassan, H. H., & Amin, M. A. (2001). Corrosion inhibition of aluminum by 1,1(lauryl amido)propyl ammonium chloride in HCl solution. *Materials Chemistry and Physics*, *70*, 64–72.

Abdel Rehim, S. S., Hazzazi, O. A., Amin, M. A., & Khaled, K. F. (2008). On the corrosion inhibition of low carbon steel in concentrated sulphuric acid solutions. Part I: Chemical and electrochemical (AC and DC) studies. *Corrosion Science*, *50*, 2258–2271.

Amara, H., Braisaz, T., Villemin, D., & Moreau, B. (2008). Thiomorpholin-4-ylmethyl-phosphonic acid and morpholin-4-methyl-phosphonic acid as corrosion inhibitors for carbon steel in natural seawater. *Materials Chemistry and Physics*, *110*, 1–6.

Amin, M. A., Abd El Rehim, S. S., & Abdel-Fatah, H. T. M. (2009). Electrochemical frequency modulation and inductively coupled plasma atomic emission spectroscopy methods for monitoring corrosion rates and inhibition of low alloy steel corrosion in HCl solutions and a test for validity of the Tafel extrapolation method. *Corrosion Science*, *51*, 882–894.

Ansari, K. R., Quraishi, M. A., & Singh, A. (2014). Schiff's base of pyridyl substituted triazoles as new and effective corrosion inhibitors for mild steel in hydrochloric acid solution. *Corrosion Science*, *79*, 5–15.

Arukalam, I. O. (2012). The inhibitive effect of hydroxyethylcellulose on mild steel corrosion in hydrochloric acid solution. *Academic Research International*, *2*, 35–42.

Ashassi-Sorkhabi, H., & Ghalebsaz-Jeddi, N. (2005). Inhibition effect of polyethylene glycol on the corrosion of carbon steel in sulphuric acid. *Materials Chemistry and Physics*, *92*, 480–486.

Badiea, A. M., & Mohana, K. N. (2008). Effect of fluid velocity and temperature on the corrosion mechanism of low carbon steel in industrial water in the absence and presence of 2-hydrazino benzothiazole. *Korean Journal of Chemical Engineering*, *25*, 1292–1299.

Baoa, Q., Zhanga, D., & Wan, Y. (2011). 2-Mercaptobenzothiazole doped chitosan/11-alkanethiolate acid composite coating: Dual function for copper protection. *Applied Surface Science*, *257*, 10529–10534.

Benchikh, A., Aitout, R., Makhloufi, L., Benhaddad, L., & Saidani, B. (2009). Soluble conducting poly(aniline-co-orthotoluidine) copolymer as corrosion inhibitor for carbon steel in 3% NaCl solution. *Desalination*, *249*, 466–474.

Bentiss, F., Bounanis, M., Mernari, B., Traisne, M., Vezin, H., & Lagrenee, M. (2007). Understanding the adsorption of 4H-1,2,4-triazole derivatives on mild steel surface in molar hydrochloric acid. *Applied Surface Science*, *253*, 3696–3704.

Bereket, G., Gretir, C. O., & Yurt, A. (2001). Quantum mechanical calculations on some 4-methyl-5-substituted imidazole derivatives as acidic corrosion inhibitor for zinc. *Journal of Molecular Structure (Theochem)*, *571*, 139–145.

Bosch, R. W., Hubrecht, J., Bogaerts, W. F., & Syrett, B. C. (2001). Electrochemical frequency modulation: A new electrochemical technique for online corrosion monitoring. *Corrosion*, *57*, 60–70.

Chen, W., Hong, S., Li, H. B., Luo, H. Q., Li, M., & Li, N. B. (2012). Protection of copper corrosion in 0.5 M NaCl solution by modification of 5-mercapto-3-phenyl-1,3,4-thiadiazole-2-thione potassium self-assembled monolayer. *Corrosion Science*, *61*, 53–62.

Cheng, S., Chen, S., Liu, T., Chang, X., & Yin, Y. (2007). Carboxymenthylchitosan as an ecofriendly inhibitor for mild steel in 1 M HCl. *Materials Letters*, *61*, 3276–3280.

del Campo, L., Perez-Saez, R. B., Gonzalez-Fernandez, L., & Tello, M. J. (2009). Kinetics inversion in isothermal oxidation of uncoated WC-based carbides between 450 and 800 °C. *Corrosion Science*, *51*, 707–712.

Deng, Sh., Li, X., & Xie, X. (2014). Hydroxymethyl urea and 1,3-bis(hydroxymethyl) urea as corrosion inhibitors for steel in HCl solution. *Corrosion Science*, *80*, 276–289.

Ehteshamzadeh, M., Shahrabi, T., & Hosseini, M. (2006). 3,4-Dimethoxy-benzaldehydethio-semicarbazone as corrosion inhibitor. *Anti-corrosion Methods and Materials*, *53*, 296–302.

El-Haddad, M. N. (2013). Chitosan as a green inhibitor for copper corrosion in acidic medium. *International Journal of Biological Macromolecules*, *55*, 142–149.

El-Haddad, M. N., & Elattar, K. M. (2012). Role of novel oxazocine derivative as corrosion inhibitor for 304 stainless steel in acidic chloride pickling solutions. *Research on Chemical Intermediates*, *39*, 3135–3149.

El-Sayed, A. (1996). A study of the inhibiting action of some polymers on the corrosion of iron in acidic media. *Corrosion Prevention and Control*, *43*, 27–34.

Fekry, A. M., & Mohamed, R. R. (2010). Acetyl thiourea chitosan as an eco-friendly inhibitor for mild steel in sulphuric acid medium. *Electrochimica Acta*, *55*, 1933–1939.

Growcock, F. B., & Jasinski, J. H. (1989). Time-resolved impedance spectroscopy of mild steel in concentrated hydrochloric acid. *Journal of Electrochemical Society*, *136*, 2310–2314.

Karakus, M., Sahin, M., & Bilgiç, S. (2005). An investigation on the inhibition effects of some new dithiophosphonic acid monoesthers on the corrosion of the steel in 1 M HCl medium. *Materials Chemistry and Physics*, *92*, 565–571.

Khaled, K. F. (2008). Guanidine derivative as a new corrosion inhibitor for copper in 3% NaCl solution. *Materials Chemistry and Physics*, *112*, 104–111.

Li, Y., Zhao, P., Liang, Q., & Hou, B. (2005). Berberine as a natural source inhibitor for mild steel in 1 M H_2SO_4. *Applied Surface Science*, *250*, 1242–1253.

Li, X. H., Deng, S. D., & Fu, H. (2009). Synergism between red tetrazolium and uracil on the corrosion of cold rolled steel in H_2SO_4 solution. *Corrosion Science*, *51*, 1344–1355.

Ma, H., Chen, S., Niu, L., Zhao, S., Li, S., & Li, D. (2002). Inhibition of copper corrosion by several Schiff bases in aerated halide solutions. *Journal of Applied Electrochemistry*, *32*, 65–72.

Machnikoval, E., Pazderova, M., Bazzaoui, M., & Hackerman, N. (2008). Corrosion study of PVD coatings and conductive polymer deposited on mild steel Part I: Polypyrrole. *Surface and Coatings Technology*, *202*, 1543–1550.

Materials Studio v 5.0, copyright Accelrys Software Inc. (2009).

Müller, B., Förster, I., & Kläger, W. (1997). Corrosion inhibition of zinc pigments in aqueous alkaline media by polymers. *Progress in Organic Coatings*, *31*, 229–233.

Mulliken, R. S. (1955). Electronic population analysis on LCA-OMO molecular wave functions. *Journal of Chemical Physics*, *23*, 1833–1840.

Obot, I. B., Obi-Egbedi, N. O., & Umoren, S. A. (2009). Antifungal drugs as corrosion inhibitors for aluminium in 0.1 M HCl. *Corrosion Science*, *51*, 1868–1875.

Okafor, P. C., Liu, X., & Zheng, Y. G. (2009). Corrosion inhibition of mild steel by ethylamino imidazoline derivative in CO_2-saturated solution. *Corrosion Science*, *51*, 761–768.

Paskossy, T. (1994). Impedance of rough capacitive electrodes. *Journal of Electroanalytical Chemistry*, *364*, 111–125.

Quraishi, M. A., & Rawat, J. (2001). Influence of iodide ions on inhibitive performance of tetraphenyl-dithia-octaaza-cyclotetradeca-hexaene (PTAT) during pickling of mild steel in hot sulfuric acid. *Materials Chemistry and Physics*, *70*, 95–99.

Refaey, S. A. M., Taha, F., & Abd El-Malak, A. M. (2004). Inhibition of stainless steel pitting corrosion in acidic medium by 2-mercaptobenzoxazole. *Applied Surface Science*, *236*, 175–185.

Sahin, M., Gece, G., Karc, F., & Bilgic, S. (2008). Experimental and theoretical study of the effect of some heterocyclic compounds on the corrosion of low carbon steel in 3.5% NaCl medium. *Journal of Applied Electrochemistry*, *38*, 809–815.

Sathiyanarayanan, S., Balakrishnan, K., Dhawan, S. K., & Trivedi, D. C. (1994). Prevention of corrosion of iron in acidic media using poly(o-methoxy-aniline). *Electrochimica Acta*, *39*, 831–837.

Singh, A. K., & Quraishi, M. A. (2010). Inhibitive effect of diethylcarbamazine on the corrosion of mild steel in hydrochloric acid. *Corrosion Science*, *52*, 1529–1535.

Solomon, M. M., & Umoren, S. A. (2010). Inhibitive and adsorption behaviour of carboxymethylcellulose on mild steel corrosion in sulphuric acid solution. *Corrosion Science*, *52*, 1317–1325.

Umoren, S. A. (2008). Inhibition of aluminium and mild steel corrosion in acidic medium using gum Arabic. *Cellulose*, *15*, 751–761.

Umoren, S. A., Solomon, M. M., Udosoro, I. I., & Udoh, A. P. (2010). Synergistic and antagonistic effects between halide ions and carboxymethylcellulose for the corrosion inhibition of mild steel in sulphuric acid solution. *Cellulose*, *17*, 635–648.

Waanders, F. B., Vorster, S. W., & Geldenhuys, A. J. (2002). Biopolymer corrosion inhibition of mild steel: Electrochemical/mössbauer results. *Hyperfine Interactions*, *139–140*, 133–139.

WHO. (1998). *Food additives and contaminants*. Geneva, Switzerland: Food additives series 40.

Wu, X. J., Ma, H. Y., & Chen, S. H. (1999). General equivalent circuits for Faradaic electrode processes under electrochemical reaction control. *Journal of Electrochemical Society*, *146*, 1847–1853.

Zhou, C., Lu, X., Xin, Z., Liu, J., & Zhang, Y. (2014). Polybenzoxazine/SiO_2 nanocomposite coatings for corrosion protection of mild steel. *Corrosion Science*, *80*, 269–275.